This is an open access article published under an ACS AuthorChoice License, which permits copying and redistribution of the article or any adaptations for non-commercial purposes.

ACSNANO www.acsnano.org

ARTICLE

All Subdomains of the Talin Rod Are Mechanically Vulnerable and May Contribute To Cellular Mechanosensing

Alexander William M. Haining,[†] Magdaléna von Essen,[‡,§] Simon J. Attwood,[†,#] Vesa P. Hytönen,[*,‡,§] and Armando del Río Hernández[*,†]

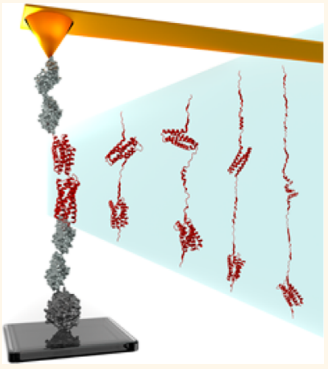
[†]Cellular and Molecular Biomechanics Laboratory, Department of Bioengineering, Imperial College London, London SW7 2AZ, United Kingdom

[‡]BioMediTech, University of Tampere, Biokatu 6, FI-33520 Tampere, Finland

[§]Fimlab Laboratories, Biokatu 4, FI-33520 Tampere, Finland

Supporting Information

ABSTRACT: **Although the relevance of mechanotransduction in cell signaling is currently appreciated, the mechanisms that drive this process remain largely unknown. Mechanical unfolding of proteins may trigger distinct downstream signals in cells, providing a mechanism for cellular mechanotransduction. Force-induced unfolding of talin, a prominent focal adhesion protein, has been demonstrated previously for a small portion of its rod domain. Here, using single-molecule atomic force microscopy (smAFM), we show that the entire talin rod can be unfolded by mechanical extension, over a physiological range of forces between 10 and 40 pN. We also demonstrate, through a combination of smAFM and steered molecular dynamics, that the different bundles within the talin rod exhibit a distinct hierarchy of mechanical stability. These results provide a mechanism by which different force conditions within the cell control a graduated unfolding of the talin rod. Mechanical unfolding of the rod subdomains, and the subsequent effect on talin's binding interactions, would allow for a finely tuned cellular response to internally or externally applied forces.**



KEYWORDS: *mechanotransduction, single-molecule force spectroscopy, steered molecular dynamics, protein mechanostability, mechanobiology*

Research in recent years has demonstrated the relevance of a cell's ability to interpret the mechanical properties of its surroundings. This ability of a cell to convert mechanical signals into signaling cascades, *i.e.*, mechanotransduction, has been shown to drive a wide variety of cellular phenomena including cancer progression and stem cell differentiation.[1,2] Despite an appreciation of the importance of these mechanical signals, the mechanisms by which cells translate them remain unknown.

One of the focus areas for finding a mechanism of cellular mechanotransduction concerns the integrin-mediated adhesions. Integrins, as transmembrane proteins, provide a connection between the interior of the cell and the extracellular matrix (ECM) that surrounds it. As anchorage points for the cell, they orchestrate the bidirectional mechanical communication of the cell with the ECM. Integrins are important not just for stable cell−ECM adhesion but also for cellular force generation and motility. As well as providing this connection, integrins help to recruit a cluster of intracellular proteins. In this process, early adhesions (focal complexes) are matured to protein-rich plaques called focal adhesions. This process is tightly regulated by mechanical signals: Contractile actomyosin cytoskeleton and adequate stiffness in the extracellular matrix are needed to drive the adhesion maturation process.[3−5] Furthermore, it is possible to control the size of the adhesion plaques by applying external force locally.[6,7] Thus, integrin-mediated adhesions have been a key area for investigations into cellular mechanotransduction. In particular, studies into the mechanosensitivity of these adhesions and how this might lead to cellular mechanotransduction have been centered on the focal adhesion protein talin.

Due to its unique and prominent position as a mechanical linkage between the ECM-bound integrins and the cellular cytoskeleton, talin has been hypothesized to be the crucial mechanosensitive molecule in focal adhesions.[8] Talin is essential for cellular spreading[9,10] and is responsible for early connections between integrin and actin cytoskeleton.[11]

Received: March 8, 2016
Accepted: July 5, 2016
Published: July 5, 2016

 © 2016 American Chemical Society

DOI: 10.1021/acsnano.6b01658
ACS Nano 2016, 10, 6648−6658

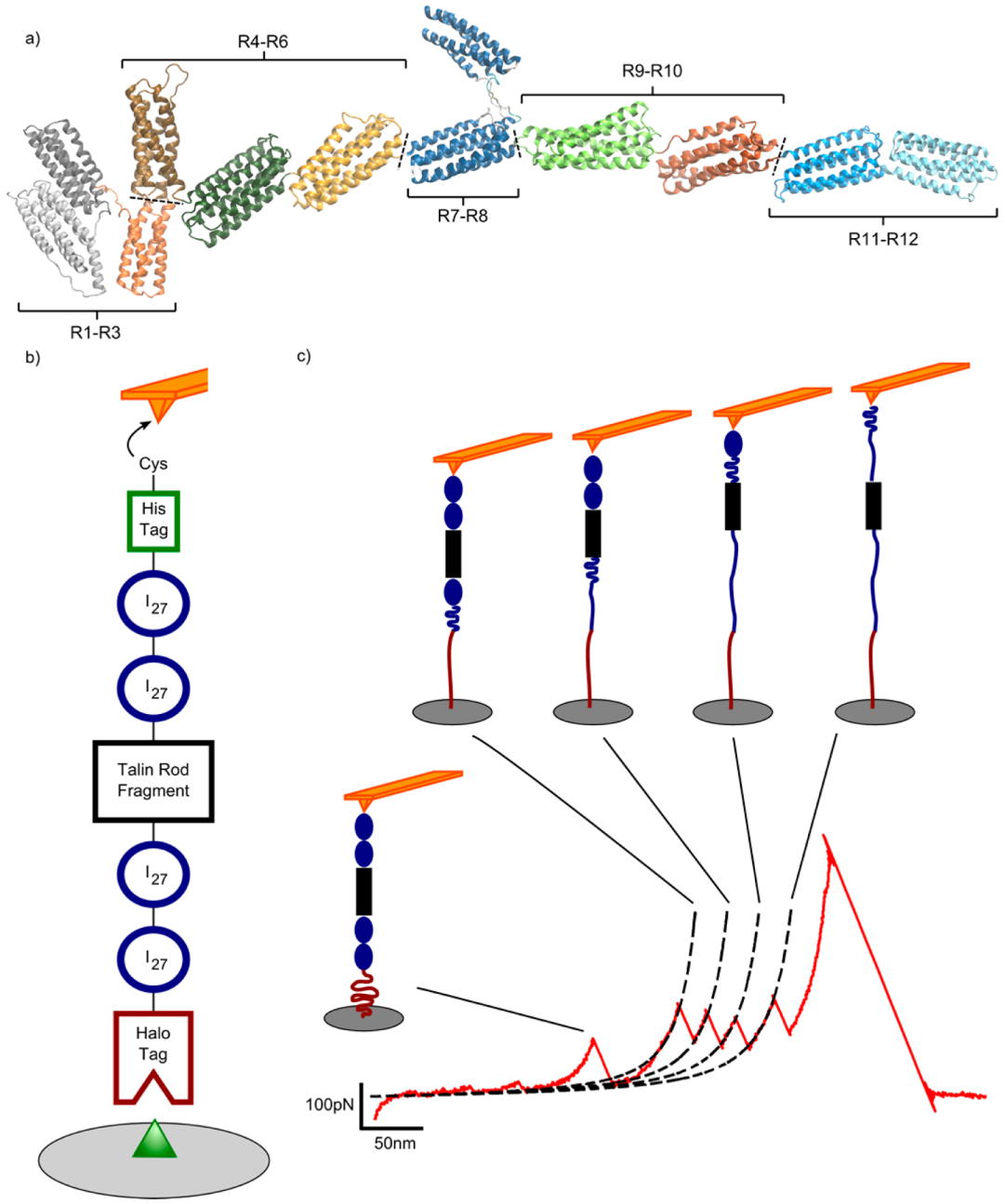


Figure 1. Talin rod polyprotein constructs for smAFM experiments. (a) Crystal structure of talin rod, showing the α-helical bundles R1−R12. The rod was separated into different fragments as indicated for the AFM experiments. (b) Schematic of the polyprotein constructs containing: the talin fragment to be investigated; four flanking I_{27} domains for fingerprinting; the HaloTag enzyme that binds to its associated ligand on the surfaces; a HisTag for protein purification; and a terminal cysteine for cantilever tip attachment. (c) Example of fingerprint used for identification. After the unfolding of the talin rod fragment, the first peak corresponds to the unfolding of the HaloTag enzyme. This is followed by the unfolding events for the four I_{27} domains, creating the characteristic "sawtooth" pattern. The final peak represents the detachment of the polyprotein from either the surface or the cantilever. The dashed lines indicate a worm-like chain model fit applied to the I_{27} unfolding events. (b, c) Not to scale.

Investigations into the mechanosensitivity of talin have so far been focused on talin's interaction with vinculin, another focal adhesion protein. Our previous studies were the first to demonstrate this mechanosensitivity, both *in silico* and experimentally. We showed that force-induced stretching of the talin rod exposes new cryptic vinculin binding sites (VBS) and increases the vinculin recruitment to the talin rod.[12,13] Similar studies by others have supported and enhanced this concept.[14,15] All these studies, however, were focused around a small, N-terminal subregion of the rod, bundles R1−R3. The compact nature of this region and the abundance of VBSs leads to the possibility that this region alone is responsible for talin's mechanosensing, while the remainder of the rod, proposed to be linear in structure, is responsible for force propagation.[16] Up until now, however, the response of this linear region to force has never been investigated.

The mechanical load applied to cellular components may vary substantially depending on the cellular substructure and the cellular event. Thus, it is possible that a subpopulation of the proteins is under high load in certain situations, when

DOI: 10.1021/acsnano.6b01658
ACS Nano 2016, 10, 6648−6658

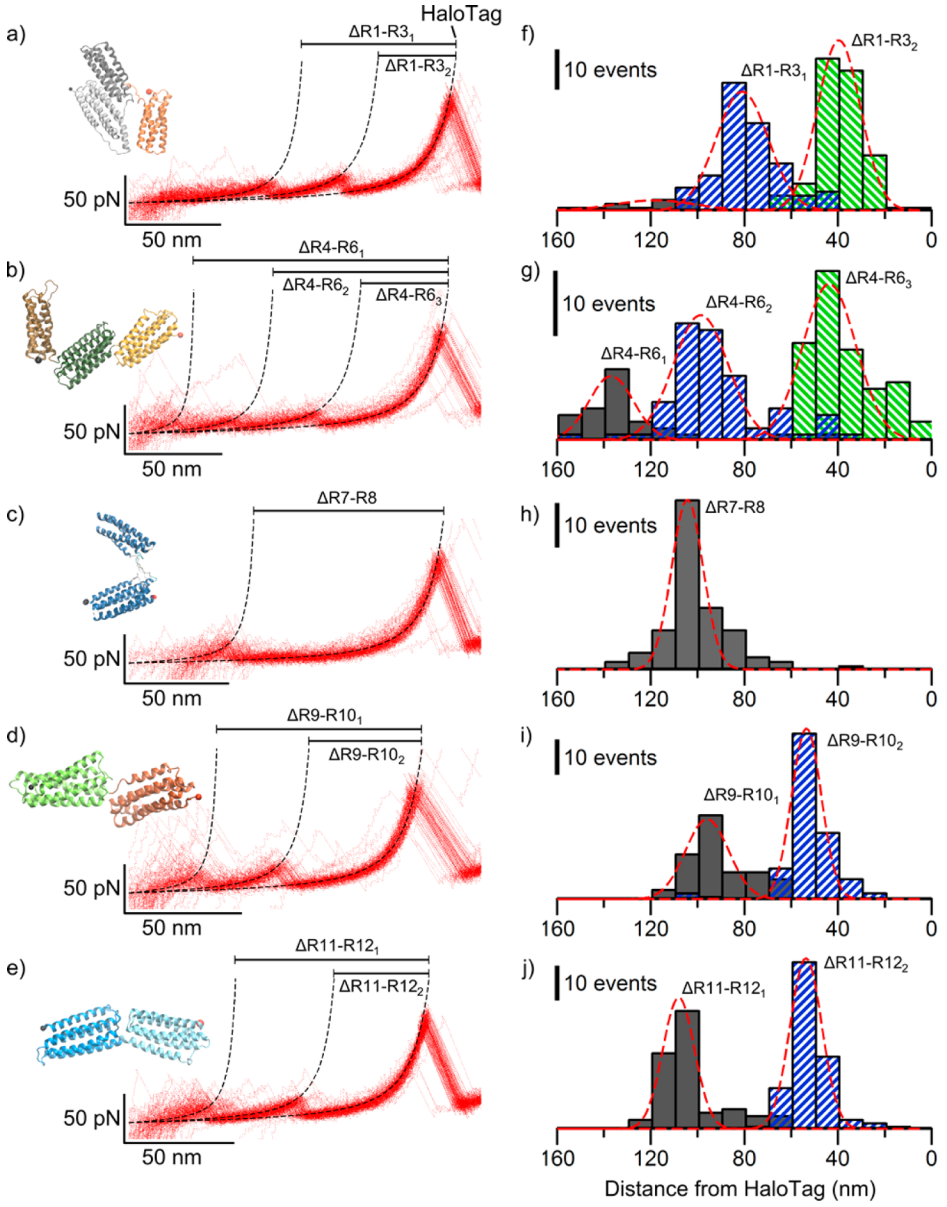


Figure 2. Unfolding pattern of talin rod fragments. (a–e) Aggregated force extension traces reveal the unfolding pattern of each fragment. The fingerprints of each trace were used for alignment, revealing the number of unfolding events and the extension associated with each. Inset: crystal structures for each fragment. Each event is fitted to the worm-like chain model (dashed lines). The method for measuring the extension of each event is also shown. (f–j) Histograms of the extensions associated with each unfolding events. The extension associated with each unfolding event was measured, using HaloTag as a reference point. The *x*-axes have been reversed so that the order of the unfolding peaks in the histogram matches the order of unfolding in the traces, *i.e.*, the furthest peak from HaloTag is the first to unfold. Red dashed lines show Gaussian fits applied to the histograms. Extension lengths are summarized in Supporting Information Table S1. (a, f) R1–R3, number of traces analyzed, n = 101. (b, g) R4–R6, n = 76. (c, h) R7–R8, n = 82. (d, (i) R9–R10, n = 91. (e, j) R11–R12, n = 103.

responsible for particular cellular functions. Experimental methods have emerged that allow measurement of these forces applied to intracellular proteins such as talin and vinculin.[9,17] The fact that talin is the most prominent candidate for consideration as a cellular mechanosensor means that the elucidation of the biomechanical properties of the full rod in response to force is indispensable to the understanding of its function. The presence of numerous relevant binding sites in the remainder of the rod (R4–R13), including six VBSs and binding sites for other proteins including RIAM, synemin and DLC1, means that the response of this region to force could have a profound effect on the modulation of talin's interactions.[18–20]

There are, however, difficulties associated with studying the full-length talin rod using single-molecule techniques. First, it is a large, amphipathic domain (~2000 aa) and as a result can be difficult to handle. Second, the length of the fully stretched talin rod domain is longer than the maximum travel distance (<1 μm) allowed by high-resolution single-molecule atomic force microscopy (smAFM) setups. Third, studies conducted on the complete rod would lose information about how the observed unfolding relates to individual bundle structures.

In this study, we circumvent these restrictions by separating the rod into smaller subdomains. These subdomains are then analyzed using a state of the art smAFM setup, combined with recent advances in single-molecule stretching techniques. The

DOI: 10.1021/acsnano.6b01658
ACS Nano 2016, 10, 6648–6658

subdomains are inserted into polyprotein constructs; these constructs contain flanking, fingerprinting molecules that allow for correct trace determination through a characteristic unfolding pattern (Figure 1).[13] The constructs also contain an N-terminal HaloTag enzyme that, when coupled to ligand-prepared surfaces, ensures that the talin subdomains are extended in the desired orientation.[21] This unique combination of smAFM techniques allows us to establish an outline of the unfolding pattern of the talin rod. We also used all-atom steered molecular dynamics (SMD) simulations on each of the individual bundles, to provide a profile for how this applied tension is rearranging these bundles at a structural level. These complementary data sets allow us to compare the relative stabilities of the bundles for the full rod and thus propose a sequence for how talin might unravel under force application *in vivo*.

RESULTS

Generation of Talin Rod Constructs. The talin rod is comprised solely of α-helical bundles, and the structures of these individual bundles have been resolved using structural biology methods. In this study, we utilized the current structural model of the full-length talin rod.[1] The talin rod consists of 62 α-helices, which then form into bundles (R1−R13), each containing four or five helices. The talin rod was first divided into five separate fragments in order to characterize their unfolding properties under force application by smAFM. The fragments were based on the best available knowledge of the organization of the bundles for the whole rod (Figure 1a): the boundaries between the fragments were placed similarly to those used to fragment the rod for the determination of the crystal structures.[16] In the case of two of the fragments, the boundaries were dictated by their structures: bundle R8 is inserted between the third and fourth helices of R7, and thus they were expressed together; and R11 and R12 share a common, elongated helix between them. The fragment R1−R3 has previously been analyzed and thus was included as a reference to those earlier works.[2] The remaining bundles, R4−R6 and R9−R10, were clustered into two fragments. R13 was excluded, as talin's primary actin binding site occurs in this bundle, and thus it is unlikely to be extended from its N and C termini. The details of the polyprotein expression plasmids are provided in Supporting Information Figure 1.

In order to improve the efficiency of data capture and analysis, these fragments were engineered into polyprotein constructs (Figure 1b). All constructs were produced in *E. coli* and purified to homogeneity according to previous protocols.[13,22] These constructs ensure that the talin fragments were extended in the correct orientation, *i.e.*, from their N and C termini. The use of an N-terminal HaloTag protein and C-terminal cysteine residue has been shown previously to provide specific, stable attachment of polyproteins to the Halo-ligand-functionalized smAFM surface and gold-coated cantilever tip, respectively.[3] The immunoglobulin domain, I_{27}, from titin has been used to provide a molecular "fingerprint" to determine valid force extension traces.[13,23] Only traces which displayed the unfolding of the HaloTag and the characteristic "sawtooth" pattern of at least three I_{27} domains were accepted for analysis (Figure 1c).

Unfolding Pattern of Talin Rod Fragments. The talin rod constructs were extended at a constant velocity (400 nm/s) in order to investigate how the individual fragments unfold. The molecular fingerprint, first used to filter for valid traces as discussed above, was then used to match traces to one another by aligning the sawtooth patterns of the I_{27} domains. These aggregated overlaid traces show that the talin rod fragments unfold in a consistent manner with defined unfolding events (Figure 2a−e). For each trace, these unfolding events were then fitted to a worm-like chain model, and the unfolding length of each event was measured, with the HaloTag peak as a reference point. Histograms of these unfolding lengths demonstrate the number of discrete unfolding events and the regular intervals at which they occur (Figure 2f−j).

For R4−R6, R9−R10, and R11−R12, the number of unfolding events is the same as the number of bundles in the fragment. This indicates that each bundle has a single dissociation event that allows it to unravel. The distances between the peaks of the histograms can be analyzed to determine the length of unfolding that occurs for each event. These lengths tend to be 10−30% shorter than the theoretical fully extended length of the amino acid chain for each bundle (Supporting Information Table S1).[24] This indicates that either the bundles partially unravel before their main dissociation event or that, after they dissociate, they still retain some of their α-helical structure.

For R1−R3, a three bundle construct, only two events were usually observed, although in several traces the anticipated three events were discernible. This apparent difference is explained by previous work on this fragment that has shown that the R3 bundle unfolds at forces as low as 5 pN, which is below the resolution of this smAFM apparatus.[15] As with the other fragments, the length of unfolding is less than the theoretical maximum length of the amino acid chains (Supporting Information Table S1).

The R7−R8 fragment is different to the others both in structure and in the unfolding pattern that it generates. In all traces only a single unfolding event occurs, despite the presence of two bundles. Additionally the unfolding length of 104 ± 7 nm is much greater than the potential unfolded length of either individual bundle (Supporting Information Table S1). This indicates that a single dissociation event results in both bundles unravelling. This notion is supported by the structural work on this fragment which demonstrated that the R8 bundle is much weaker than the R7 and stabilized by its insertion between the third and fourth helices of R7.[5] It can therefore be surmised that once the R7 bundle is ruptured and begins to unravel, the instability of the R8 bundle allows it to be unravelled without a second dissociation event.

Talin Rod Bundles Dissociate over a Range of Forces. As well as illuminating the pattern of fragment unfolding, the force extension data can be analyzed to determine the force associated with each unfolding event. These forces were combined into histograms that demonstrate the range of forces involved (Figure 3a−e). The unfolding of all talin rod fragments seems to occur over a range of forces between 10 and 40 pN. Within that range, individual unfolding events seem to occur at specific forces, indicating that different bundles may exhibit different levels of mechanical stability (Supporting Table S1). This indicates that talin may consist of mechanical elements with a range of mechanical stabilities, such as has been proposed previously for fibronectin.[25] We therefore performed further analyses to dissect the mechanical characteristics of the talin rod components.

SMD and AFM Analysis Reveal Hierarchy of Bundle Stability. Constant velocity end-to-end pulling simulations at 0.1 nm/ns and 2 nm/ns revealed that all tested talin rod

DOI: 10.1021/acsnano.6b01658
ACS Nano 2016, 10, 6648−6658

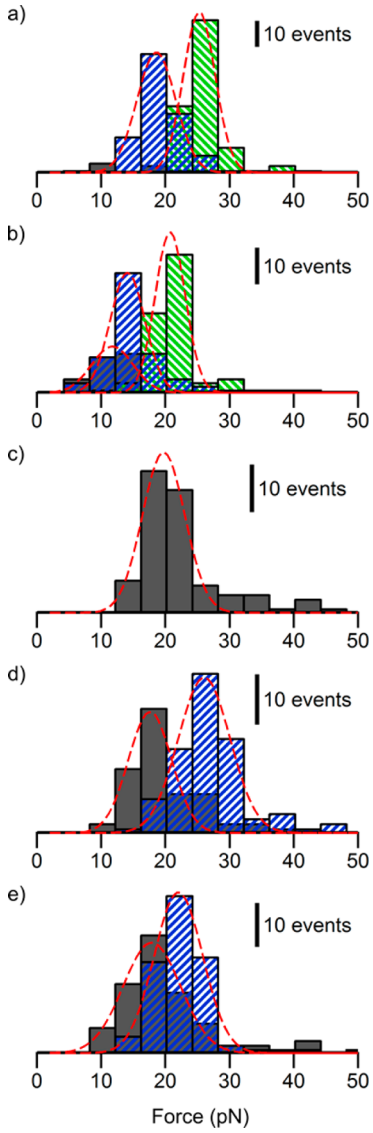


Figure 3. Unfolding force of talin rod fragments using smAFM. (a–e) Histograms of the unfolding force for each event. Gray bars represent the unfolding event closest to HaloTag. Blue bars, where applicable, show the next event further from HaloTag. Finally green bars show the first unfolding event, and furthest from HaloTag, for those traces exhibiting three events. Red dashed lines show Gaussian fits applied to the histograms. Forces are summarized in Supporting Information Table S1. (a) R1–R3. (b) R4–R6. (c) R7–R8. (d) R9–R10. (e) R11–R12.

domains unfold over a range of forces (Figure 4). The constant velocity simulations at 2 nm/ns allowed us to obtain a comprehensive picture of the unfolding pathway within 20 ns simulation. Three simulations were performed for each of the bundles to ensure the reproducibility of the traces obtained (Supporting Information Figure S3). Simulations at 0.1 nm/ns focused on the initial breaking of the domains over approximately 40 ns. This lower velocity pulling was used to test the method sensitivity and the impact of the velocity on the final force magnitude, rather than for a comparison of trajectories. Overall, similar patterns of unfolding force magnitude were observed for both tested velocities. The pulling rates used for these simulations were much greater than physiological, with the expectation that pulling at speeds closer to those expected *in vivo* would result in dramatically lower forces, as revealed by the smAFM measurements.

Due to the character of the simulations, calculated unfolding forces from SMD are only relative and cannot be directly compared to the experimental unfolding forces. Despite the large differences in force magnitude, the unfolding trajectories illustrate very similar unfolding dynamics over the tested domains (Figure 5). Moreover, small differences in structural changes result in large changes in the calculated force magnitude. Hence, SMD unfolding force is used here only for pattern analysis and talin rod domain stability classification, but not for providing predictions for the absolute unfolding force. This is a similar approach to that presented in the work by Craig *et al.* concerning the stability of fibronectin Ig domains.[25] It is also good to keep in mind that the cellular processes may happen in the time frame of milliseconds to hours, not reachable by all-atom simulations.

Based on the relative force magnitude and unfolding trajectories, we have classified the tested talin α helix bundles into three stability groups: weak, intermediate, and strong. The weak class contains the easily unfolding four-helix bundles R3 and R4. The R3 bundle contains a belt of polar residues in its hydrophobic core unique among the talin rod bundles. This polar pattern may cause R3 destabilization and unfolding under low mechanical load. Previous studies showed that replacement of the polar belt residues by hydrophobic amino acids increased the mechanical stability of R3.[15,16] Bundle R4 also unfolded gradually without noticeable resistance in SMD. In all three 2 nm/ns simulations, the helicity in H2 (Ala960 – Pro964) and H3 (Pro996 – Met1000) of R4 was greatly disturbed by twisting and bending. This effect was observed during pulling simulations, however the areas were not affected by the mechanical force directly. Interestingly, such proline occurrence is rather uncommon across other talin helices. Furthermore, both proline residues are highly conserved between species for both talin-1 and talin-2, as determined by multiple sequence alignment (Supporting Information Table S2). The weak class additionally contains two five-helix bundles, R6 and R10, which unfold under low force in SMD. Both R6 and R10 bundles have helix H1 considerably shorter compared to other bundle helices. This may contribute to the lower domain mechanostability. The short H1 was separated in both domains early in the simulation followed by gradual unfolding of H5 at the C terminal end. In both cases we have observed a 3-helix intermediate (H2–H4) stable between approximately 8 and 11 ns for R6 and approximately 9 and 12 ns for R10 (Figure 5). Whether this intermediate represents a functionally important state remains unclear.

The intermediate class contains domains R7, R11, and R12 with domain R7 fluctuating at the border of the soft and intermediate classes during the first 9 ns of 2 nm/ns simulation. All domains in this class consist of five-helix bundles where all the helices have similar lengths. In the R11 bundle, the highly conserved residue Met2121 in H5 (the long connecting helix between R11 and R12) was identified as a possible gatekeeper in all three simulations. Met2121 is located in the IBS2-A region[26] with its hydrophobic side-chain pointing toward the hydrophobic core of R11. It creates nonpolar contacts with H2 and H4 and possibly contributes to the stability of the bundle and thus maintains the IBS2-A. Similarly to unfolding trajectories of R6 and R10, we have observed possible 3-helix intermediates consisting of H2–H4 core also in R11 and R12 simulations (Figure 5).

DOI: 10.1021/acsnano.6b01658
ACS Nano 2016, 10, 6648–6658

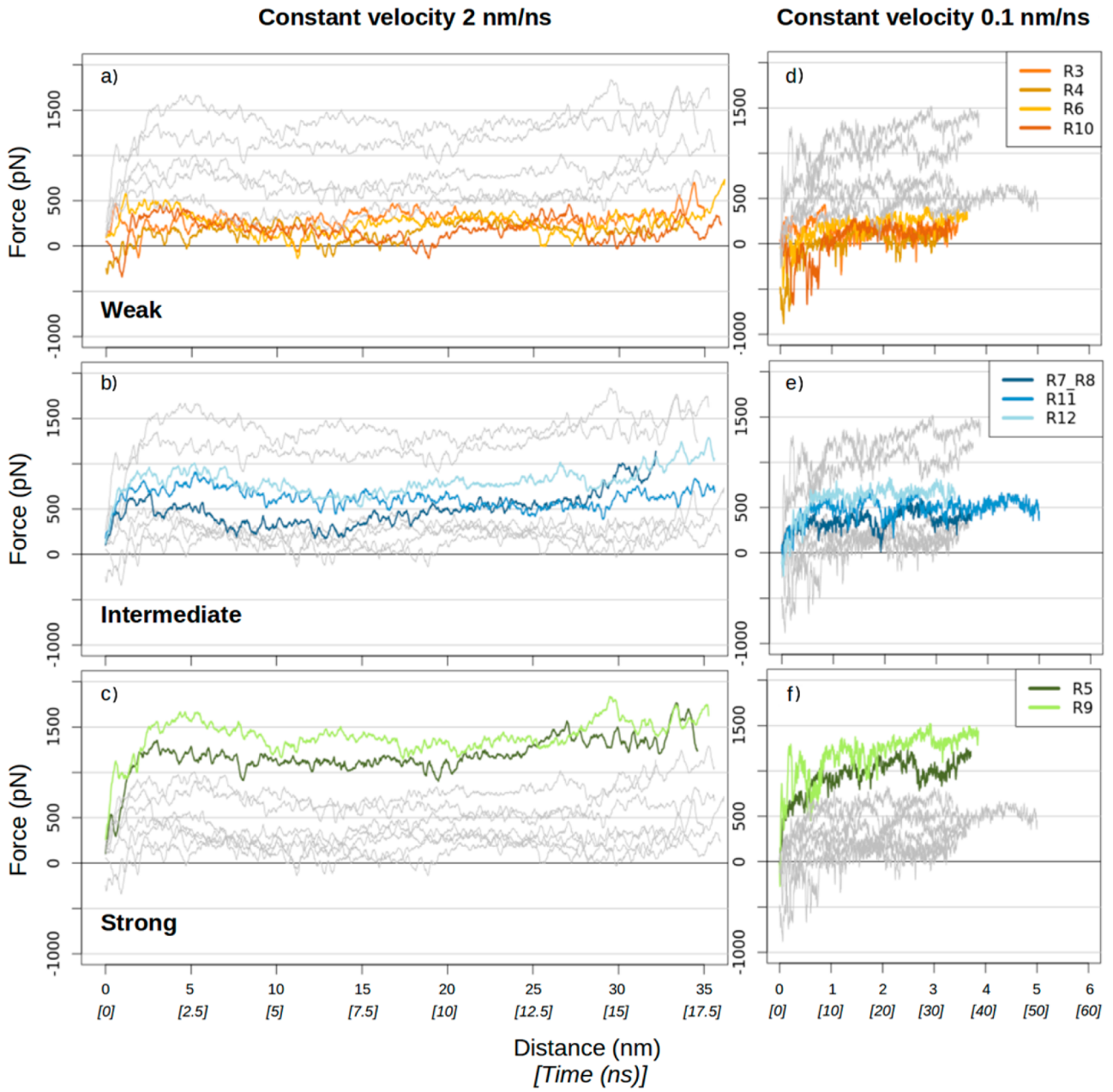


Figure 4. Unfolding force magnitude (pN) of talin rod domains in SMD. (a−c) Force against simulation time during constant velocity pulling at 2 nm/ns. (d−f) Force against simulation time during constant velocity pulling at 0.1 nm/ns. Gray lines visualize the force magnitude for all bundles. The tested rod domains show varying mechanical stability represented by different unfolding force magnitude. All rod domains are classified into three groups which are color highlighted in separate plots against the complete data set. (a, d) Weak class (orange) contains R3, R4, R6, and R10 bundles unfolding under maximum unfolding force 500pN; (b, e) intermediate class (blue) contains bundles R7, R11, and R12 unfolding between 500 and 1000pN; (c, f) strong class (green) with R5 and R9 bundles with unfolding force over 1000 pN. Similar classification was observed for both simulation settings at 0.1 nm/ns and 2 nm/ns velocity.

Finally, the strong group contains domains R5 and R9. Both of these two bundles are five-helix domains with similar helix lengths. Furthermore, in strong bundles, additional characteristic twisting of the helices around the bundle axis was observed in structural alignments when compared to the bundles of intermediate class. (Supporting Information Figure S2b). Greater displacement of helix ends at the bundle top and bottom was observed for R9 bundle, which also exhibits the greatest mechanical stability. On the other hand the smallest differences between the top and bottom helix positions can be seen for bundle R11 which is the softest of the presented bundles (R5, R9, R11, R12). Such specific twisting of the bundle is likely to increase the contact areas between its helices and increase the unfolding force demand.

To further investigate the differences of the strong (R9) and intermediate (R11) bundles, we performed individual helix alignment against an ideal α-helix. We observed that the helicity between the two bundles is affected. The average root-mean-square deviation (RMSD) of atomic positions of structural alignments was 1.810 Å for R9 and 1.599 Å for R11, suggesting that α-helices of R9 bundles are more deformed compared to R11 helices. We identified two residues which may be important for the R9 bundle stability, namely Leu1668 in H1 and Met1803 in H5. These highly conserved residues create

DOI: 10.1021/acsnano.6b01658
ACS Nano 2016, 10, 6648−6658

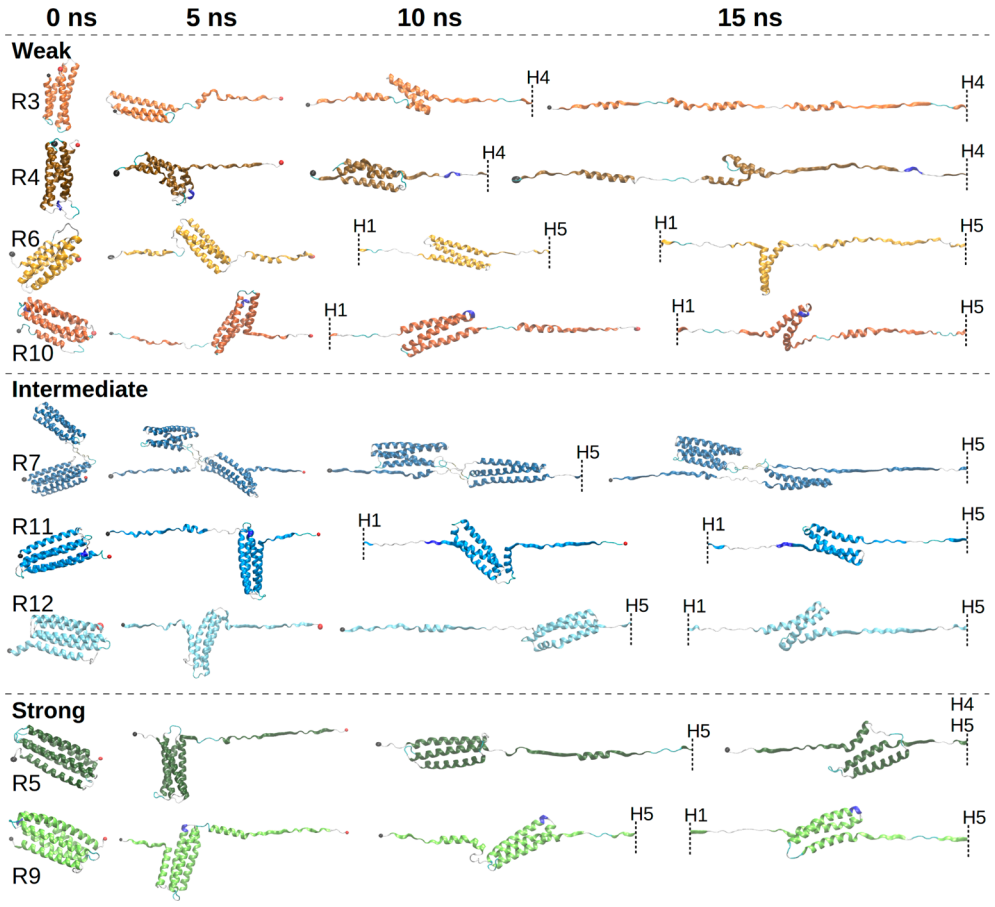


Figure 5. Representative structure snapshots of talin rod domains. Structure snaps were captured at 0, 5, 10, and 15 ns of the constant velocity pulling at 2 nm/ns. The three stability groups (weak, orange; intermediate, blue; strong, green) show mild yet distinct differences in the domain unfolding. Fully unfolded helices are cut away and presented by dashed line with a helix identifier.

large hydrophobic contacts with the core of R9. Furthermore, the Met1803 residue is located in close proximity to the R9-R8 interface as well as the interface between R9 and the talin head subdomain, F3, and may contribute to the stability of the autoinhibition conformation.[27,28]

The AFM force data support this proposed hierarchy of bundle stabilities. Based on the SMD classification, R4−R6 contain two bundles from the weak group, R4 and R6, and one strong bundle, R5. By AFM, we see two unfolding events occurring at a lower force (<20 pN) with one event at a higher force (>20 pN), well in agreement with the SMD (Figure 3b). In case of R9-R10, SMD proposes one weak bundle and one strong, and indeed, AFM demonstrates one lower force unfolding event and one with a higher force (Figure 3d). Finally, in the R11−R12 consisting of two bundles of intermediate strength according to SMD, both unfolding events seem to occur at a similar force regime (Figure 3e). Thus, there is excellent agreement between the mechanical stabilities derived from the bundle structures and those observed experimentally.

DISCUSSION

The strong links between talin and a cell's mechanosensitivity have highlighted the need for a thorough understanding of its force response. Single-molecule studies focusing on the R1−R3 region of the rod have demonstrated the basic mechanisms of this mechanosensitivity. It has been shown that unfolding of this region can occur at forces as low as 5 pN and that this unfolding leads to an increase in affinity for vinculin.[13,15] Despite the comparative lack of previous molecular investigations on the remainder of the rod, cellular studies have indicated that the regions R4−R12 may be actively involved in talin's mechanosensing. A study that measured the distance between talin's N- and C-termini showed that this length varied between 50 and 350 nm.[29] This increase in length would require the unfolding of more than just the R1−R3 region, as this region alone could only contribute up to 150 nm of added length. Additionally, super-resolution microscopy of focal adhesions has shown that vinculin binding occurs along the full rod, including R4−R13,[30] and this indicates that the cryptic VBSs of the full rod are being revealed through structural rearrangement. It is thus important to fully understand the mechanical hierarchy of the talin rod substructures in order to enable further studies to better understand the physiological and pathological role of talin.

Here we have shown that the bundles R4−R12 are vulnerable to mechanically induced structural rearrangement comparable to R1−R3. The application of force to these bundles results in characteristic unfolding events; these events are followed by extension that suggests substantial unfolding of the helical bundle structures. The unfolding of these additional bundles explains how the N−C terminal length varies in cells and also provides a mechanism by which the cryptic binding sites in these bundles become activated. Our data and techniques may be used in the future to design talin mutants of varying mechanical stability in order to evaluate the

DOI: 10.1021/acsnano.6b01658
ACS Nano 2016, 10, 6648−6658

contribution of talin-mediated mechanosensing in cellular differentiation or developmental biology processes.

In order to fully appreciate talin's role in cellular mechanotransduction, we have highlighted that force-induced structural rearrangement occurs in the whole rod domain. Crucially this occurs within a physiological force range. Recent advances in combined single-molecule cellular studies have revealed the forces acting on talin and other focal adhesion proteins. Single integrin molecules have been shown to experience forces up to 40 pN in magnitude. Additionally cells require this level of tension to be applied to integrins in early adhesion formation in order for the cells to adhere correctly.[31,32] When tension sensors were inserted into the talin molecule itself it was shown that the majority of talin molecules experience tension >7 pN with a proportion experiencing >10 pN.[9] In light of this cellular data, it is interesting that we see that all bundles in the rod unfold at forces in the 15−30 pN range, within the physiological range of forces applied to focal adhesions *in vivo*. Importantly, one may assume that the unfolding force predicted by AFM is the upper limit needed for the unfolding *in vitro*, as the retraction rate used, 400 nm/s, was higher than the accepted physiological actin retraction rate of 50−100 nm/s.[33] For comparison, Yao *et al.*, when using magnetic tweezers with a loading rate of 5 pN/s, found that the stronger bundles in R1−R3 unfolded at 12 pN and 20 pN, which compares to 19 ± 3 pN and 25 ± 2 pN for our data.[15] The loading or retraction rate affects the force of an unfolding event, with lower rates resulting in lower unfolding forces.[34] Given that our retraction rate is higher than physiological and the experiments of Yao *et al.* were conducted at the lower end or below physiological rates, it is likely that *in vivo* the unfolding forces of the talin bundles lie in the narrow range between our values.

Within this physiological range, a hierarchy of bundle stability can be observed as demonstrated by both the SMD simulations and smAFM unfolding. Stronger bundles unfold at consistently higher forces than the weaker bundles. This means that the full talin rod possesses a graduated response to force. Lower forces applied to the rod unfold only the weakest bundles, and as the force increases, first the intermediate and finally the strong bundles unfold, revealing or destroying appropriate binding sites in the unfolded domains (Figure 6).

The presence of cryptic VBSs along the rod and vinculin's importance in regulating focal adhesion pathways means that talin's graduated force response could result in a similarly graduated cellular response to force. Vinculin natively exists in an autoinhibited form where its head interacts with the tail domain. The binding of talin's VBSs with vinculin breaks this autoinhibition and thus releases the vinculin tail, which consequently interacts with actin and numerous other focal adhesion and cytoskeletal proteins.[35] Thus, increasing the force on talin could lead to greater unfolding of bundles, increased activation of vinculin, and therefore amplified vinculin-dependent downstream signaling.

This simple framework for mechanotransduction outlined above ignores the potential involvement of talin's additional binding partners. The bundles that we have investigated contain binding sites for numerous structural and signaling proteins including, RIAM, synemin, and deleted in liver cancer 1 (DLC1). RIAM assists in targeting talin to plasma membranes, through its interaction with talin and Rap1.[18] DLC1 is a potent tumor suppressor protein whose action involves the down-regulation of RhoA activity and thus reduces the contractility of

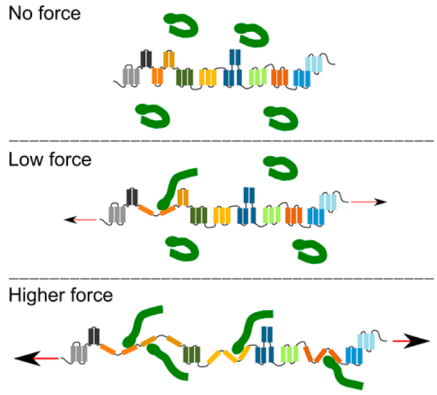


Figure 6. Cellular mechanotransduction as a result of graduated talin rod unfolding. Without force, the talin rod remains fully structured, and no VBSs are available. Under low-force regimes, only the very weakest bundle, R3, unfolds revealing its VBS. This activates one vinculin molecule, releasing it from its autoinhibited state. As the force applied to talin increases, more bundles are unfolded, revealing more VBSs and thus activating an increasing number of vinculin molecules. The helical bundles have been colored to reflect the mechanical hierarchy shown in Figure 4. This schematic represents a simplified version of vinculin-mediated talin mechanosensitivity. The process *in vivo* is likely to include additional binding partners and more complex modes of force application and unfolding.

cells.[36] The binding sites of these proteins overlap the locations of VBSs and thus are thought to compete for binding.[16,20] In the case of RIAM, it is expected that the bundled helical structure favors RIAM binding, whereas the disruption of the bundle leads to a greater affinity for vinculin. Thus, the influence of a range of physiological forces on talin's structure may modulate switching between favoring different binding partners to control cellular function. The binding to DLC1 and RIAM reduces contractility and increases the formation of lamellipodium,[37,38] whereas the presence of vinculin is a hallmark of more stable, mature adhesions. This process of mechanotransduction, through the exposure or disruption of binding sites, may be only one of the methods by which talin's behavior is controlled by force. Recent work in *Drosophila* development has shown the importance how two talin molecules are orientated with respect to each other when in its dimerized form.[39] Crucially, simulations have demonstrated that the orientation of the talin dimer, as dictated by its N-terminal dimerization domain, is controlled by the application of force.[40] Thus, the ability of talin to interpret forces and consequently direct cell behavior may be occurring on multiple levels of structure.

The current study communicates the role of α-helical proteins in mechanosensing. It is worth noting that the vast majority of the previous studies focusing on mechanostability of the proteins are conducted using proteins mainly containing β-sheet secondary structures. α-Helical proteins, however, may represent a highly important class of mechanosensing proteins.[41,42] Interestingly, twisting of the helical structures around the bundle axis, similar to our description for the R9 bundle, can be observed for other α-helical proteins with an important role in mechanobiology. A broad variety of helical organization and degree of bundle twist can be detected over many mechanotransducers and structural proteins, such as spectrin, α-actinin, or nuclear lamin. However, the role of such structural characteristics on the mechanostability is yet to be

DOI: 10.1021/acsnano.6b01658
ACS Nano 2016, 10, 6648−6658

fully determined. The unique properties of the α-helices render some challenges in terms of the SMD. The helices stretch substantially upon unfolding, and the interactions between helices are dictated by entropy-mediated interactions, thus causing possible bias in the relevance of the absolute force determined. However, despite these limitations, we propose that SMD simulations are useful and reliable for the determination of relative mechanical stabilities, especially when used in conjunction with smAFM, a combination that has not been provided previously. It may be possible to further develop the SMD methodology to better serve the needs of α-helical protein research, but this is out of the scope of the current study. It is also worth noting that although the separation of the rod into fragments facilitated the study of its biomechanical properties, it is possible that interactions between bundles in separate fragments may alter their stability and behavior under load. Future studies will be required to elucidate the complete picture of the unfolding of the full-length talin rod and precisely how this integrates with its role in mechanotransduction.

CONCLUSIONS

The combination of SMD and AFM single-molecule experiments provide a valuable insight into the molecular behavior and biological mechanisms. In this study, it has revealed the range of forces over which the entire talin rod unfolds and the hierarchy of mechanical stability that the different bundles exhibit. While the contribution of these methods for biological predictions and clinical significance discovery is indisputable, it is a simplified representation of the complex biological system and does not take into account the other cellular components and the close proximity of the lipid bilayer. However, as compared to cellular experiments, the benefit is that we can exclude the contribution of other factors and thus enable better testing systems to be built using cell and animal models.

Based on the results of our study, we hypothesize that talin acts as a delicate force meter sensitive to a range of small mechanical forces. Such fine mechanosensing could control the affinity switch toward ligands triggering biochemical cascades that lead to strong surface adhesion or active spreading and locomotion. Given that the observed range of bundle stabilities depends on small structural differences, we also propose that changes in the mechanical stability of the talin rod bundles could be modulated by a small number of single-point mutations. These alterations may lead to misinterpretation of the mechanical impulse and an aberrant cellular response. Hypothetically, such false interpretation could lead into pathological changes in cell differentiation and tissue growth leading to disease development.[43] Work by others has shown that talin expression is vital for cell differentiation and embryogenesis.[2,44] The effect of mutations on talin mechanostability and cellular behavior, however, has yet to be demonstrated. In the light of this discussion, it is clear that understanding the principles and mechanisms of talin-mediated mechanotransduction may provide crucial insights into the biology in health and in disease.

METHODS

Generation of Polyprotein Constructs. The talin fragment polyprotein constructs, including flanking I_{27}, were synthesized and cloned in to pFN18a. The polyproteins were expressed in *E. coli* BL21-CodonPlus (DE3)-RILP competent cells, using the T7 promoter present in the plasmid. Protein expression was induced with IPTG when the culture reached an $OD_{600\ nm}$ of 0.6. Cells were lysed with lysozyme and sonication before being purified with Ni-NTA beads in a batch process. The eluted proteins were analyzed for purity with SDS-PAGE. Final concentration of protein used for experiments was 1−10 μg/mL.

Preparation of Ligand-Functionalized Surfaces. Glass coverslips were functionalized with the chloroalkane ligand to HaloTag as previously described.[21] The glass coverslips were first cleaned using Helmanex III (1% in water), acetone ,and ethanol washes. The surfaces were then prepped with O_2 plasma cleaning for 15 min. Surfaces were then silanized using (3-aminopropyl)trimethoxysilane, diluted to 1% in ethanol. Surfaces were then washed with ethanol and then dried with N_2. These amine-functionalized surfaces were then incubated with 10 mM succinimidyl-[(*N*-maleimidopropionamido)-tetracosaethylene glycol] ester (SMPEG24 − Thermo) diluted in 100 mM borax buffer (pH 8.5) for 1 h. The final step involved incubating the surfaces overnight with 10 mM HaloTag Thiol O4 ligand in the same buffer. The surfaces were quenched with 50 mM 2-mercaptoethanol in water.

AFM Experiments and Analysis. We used a commercial AFS-1 from Luigs & Neumann, GmbH, based on a device developed at the Fernandez Lab, Columbia University.[22] The cantilevers used were gold-coated OBL-10 levers from Bruker. The spring constants varied between 4 and 10 pN/nm as measured by equipartition theorem with the appropriate adjustments for cantilever geometry.[45,46] Around 20 μL of protein solution was incubated on functionalized coverslips for 30 min prior to the experiments to allow for HaloTag binding. The cantilever was pressed into the surface with a force of ∼300 pN to bind the cantilever to the polyprotein. Force extension experiments were conducted at 400 nm/s retraction rate. Data analysis was carried out using Igor Pro (Wavemetrics), where the worm-like chain model was applied.

SMD Simulation. In SMD, all tested talin rod domains were analyzed for mechanical stability separately with the exception of R7. Bundle R7 was modeled together with inseparable R8 domain. The following structures from RCSB Protein Data Bank (RCSB PDB) were used for the models; R3 (id 2L7A residues 796−909), R4 (id 2LQG), R5 (id 2L7N), R6 (id 2L10), R7−R8 (id 2X0C), R9 (id 2KBB), R10 (id 2KVP), R11 (id 3DYJ residues 1975−2145), R12 (id 3DYJ residues 2131−2291). Anchors and extra sequence parts used for structure crystallization were removed from all analyzed models in PyMOL ver.1.4.1.

SMD simulations were performed using Gromacs ver 4.6.7 at the Sisu supercomputer, CSC, Finland.[47,48] For each model, the CHARMM27 force field and explicit TIP3P water model in 0.15 M KCL neutral solution were used. Pulling vector was set between Cα of first and last residue of appropriate domain. Consequently each structure was oriented according to the pulling vector in z direction of the simulation box. Each model was minimized to 100,000 steps and equilibrated for 1 ns. The system equilibration was monitored by following the temperature, pressure, and density parameters over time. The structure equilibration was assessed by plotting the backbone RMSD value for each bundle subjected to pulling throughout the equilibration, *i.e.*, R8 was omitted from the analysis. For all bundles the RMSD reached plateau within 0.8 ns of 1 ns equilibration. All equilibration parameters were stabilized within 1 ns for all modeled structures. Simulations were performed with constant velocity pulling at 0.1 nm/ns (n = 1) and 2 nm/ns (n = 3). All simulations were run at NPT conditions with Berendsen thermostat and Berendsen barostat. Temperature control was set to 310 K, time constant to 0.1 ps, pressure control to 1.0 bar, and compressibility to 4.5×10^{-5} bar. Temperature and pressure controls were applied separately for protein and solution parts. Furthermore, equilibration was performed at isotropic conditions while pulling at semi-isotropic conditions where pressure control was turned off in the pulling direction (z-axis). The conditions used were validated by using extensive set of simulations. Spring constant was set to 1000 kJ/mol nm.[2]

Force of the spring was calculated according to $F = k_{spring}(x_{ideal\ t} + x_0 - x_t)$, where k is the spring constant, $x_{ideal\ t}$ is the ideal elongation with velocity at time point, x_0 is the pulling vector length at time = 0,

DOI: 10.1021/acsnano.6b01658
ACS Nano 2016, 10, 6648−6658

and x_t is the pulling vector length at time point. Resulting trajectories were analyzed with VMD ver 1.9.1 at 100 ps time window.[49] An average of 10 force values was presented to minimize fluctuation and eliminate noise caused by low time step (2 fs) and sampling (1000) setting for data collection and additional 5 window stride load setting in VMD analysis.

ASSOCIATED CONTENT

Supporting Information

The Supporting Information is available free of charge on the ACS Publications website at DOI: 10.1021/acsnano.6b01658.

A partial vector map for the polyprotein plasmids is included in Figure S1. Summaries of all smAFM unfolding lengths and forces are available in Table S1. A figure highlighting the extra twisting in certain bundles is provided in Figure S2. Further simulations for each of the bundles are included in Figure S3. The list of isoforms and species used for the multiple sequence alignment is detailed in Table S2 (PDF)

AUTHOR INFORMATION

Corresponding Authors

*E-mail: vesa.hytonen@uta.fi.

*E-mail: a.del-rio-hernandez@imperial.ac.uk.

Present Address

#Cambridge University Nanoscience Centre, University of Cambridge, CB3 0FF, Cambridge, United Kingdom

Notes

The authors declare no competing financial interest.

ACKNOWLEDGMENTS

This work was supported by the European Research Council (grant 282051 awarded to A.D.R.H.) and the Academy of Finland (grants 290506, 273192, 136288 awarded to V.P.H). We acknowledge CSC, Center for Scientific Computing, Espoo, Finland for the supercomputing resources. We thank the University of Tampere for their financial support *via* TGPBB graduate school. We would like to acknowledge the contributions of J. Fernandez, A. Rivas-Pardo, I. Popa, and C. Badilla of the Fernandez Lab and R. Perez-Jimenez of the Nanobiomechanics Group and thank them for their insight and assistance with the smAFM and cloning experiments.

REFERENCES

(1) Paszek, M. J.; Zahir, N.; Johnson, K. R.; Lakins, J. N.; Rozenberg, G. I.; Gefen, A.; Reinhart-King, C. A.; Margulies, S. S.; Dembo, M.; Boettiger, D.; Hammer, D. A.; Weaver, V. M. Tensional Homeostasis and the Malignant Phenotype. *Cancer Cell* **2005**, *8*, 241−254.

(2) Engler, A. J.; Sen, S.; Sweeney, H. L.; Discher, D. E. Matrix Elasticity Directs Stem Cell Lineage Specification. *Cell* **2006**, *126*, 677−689.

(3) Choquet, D.; Felsenfeld, D. P.; Sheetz, M. P. Extracellular Matrix Rigidity Causes Strengthening of Integrin-Cytoskeleton Linkages. *Cell* **1997**, *88*, 39−48.

(4) Balaban, N. Q.; Schwarz, U. S.; Riveline, D.; Goichberg, P.; Tzur, G.; Sabanay, I.; Mahalu, D.; Safran, S.; Bershadsky, A.; Addadi, L.; Geiger, B. Force and Focal Adhesion Assembly: A Close Relationship Studied Using Elastic Micropatterned Substrates. *Nat. Cell Biol.* **2001**, *3*, 466−472.

(5) Han, S. J.; Bielawski, K. S.; Ting, L. H.; Rodriguez, M. L.; Sniadecki, N. J. Decoupling Substrate Stiffness, Spread Area, and Micropost Density: A Close Spatial Relationship between Traction Forces and Focal Adhesions. *Biophys. J.* **2012**, *103*, 640−648.

(6) Riveline, D.; Zamir, E.; Balaban, N. Q.; Schwarz, U. S.; Ishizaki, T.; Narumiya, S.; Kam, Z.; Geiger, B.; Bershadsky, A. D. Focal Contacts as Mechanosensors: Externally Applied Local Mechanical Force Induces Growth of Focal Contacts by an Mdia1-Dependent and Rock-Independent Mechanism. *J. Cell Biol.* **2001**, *153*, 1175−1185.

(7) Galbraith, C. G.; Yamada, K. M.; Sheetz, M. P. The Relationship between Force and Focal Complex Development. *J. Cell Biol.* **2002**, *159*, 695−705.

(8) Kanchanawong, P.; Shtengel, G.; Pasapera, A. M.; Ramko, E. B.; Davidson, M. W.; Hess, H. F.; Waterman, C. M. Nanoscale Architecture of Integrin-Based Cell Adhesions. *Nature* **2010**, *468*, 580−U262.

(9) Austen, K.; Ringer, P.; Mehlich, A.; Chrostek-Grashoff, A.; Kluger, C.; Klingner, C.; Sabass, B.; Zent, R.; Rief, M.; Grashoff, C. Extracellular Rigidity Sensing by Talin Isoform-Specific Mechanical Linkages. *Nat. Cell Biol.* **2015**, *17*, 1597−1606.

(10) Theodosiou, M.; Widmaier, M.; Bottcher, R. T.; Rognoni, E.; Veelders, M.; Bharadwaj, M.; Lambacher, A.; Austen, K.; Muller, D. J.; Zent, R.; Fassler, R. Kindlin-2 Cooperates with Talin to Activate Integrins and Induces Cell Spreading by Directly Binding Paxillin. *eLife* **2016**, *5*, 24.

(11) Jiang, G. Y.; Giannone, G.; Critchley, D. R.; Fukumoto, E.; Sheetz, M. P. Two-Piconewton Slip Bond between Fibronectin and the Cytoskeleton Depends on Talin. *Nature* **2003**, *424*, 334−337.

(12) Hytonen, V. P.; Vogel, V. How Force Might Activate Talin's Vinculin Binding Sites: Smd Reveals a Structural Mechanism. *PLoS Comput. Biol.* **2008**, *4*, e24.

(13) del Rio, A.; Perez-Jimenez, R.; Liu, R. C.; Roca-Cusachs, P.; Fernandez, J. M.; Sheetz, M. P. Stretching Single Talin Rod Molecules Activates Vinculin Binding. *Science* **2009**, *323*, 638−641.

(14) Lee, S. E.; Kamm, R. D.; Mofrad, M. R. K. Force-Induced Activation of Talin and Its Possible Role in Focal Adhesion Mechanotransduction. *J. Biomech.* **2007**, *40*, 2096−2106.

(15) Yao, M. X.; Goult, B. T.; Chen, H.; Cong, P. W.; Sheetz, M. P.; Yan, J. Mechanical Activation of Vinculin Binding to Talin Locks Talin in an Unfolded Conformation. *Sci. Rep.* **2014**, *4*, 4610 DOI: 10.1038/srep04610.

(16) Goult, B. T.; Zacharchenko, T.; Bate, N.; Tsang, R.; Hey, F.; Gingras, A. R.; Elliott, P. R.; Roberts, G. C. K.; Ballestrem, C.; Critchley, D. R.; Barsukov, I. L. Riam and Vinculin Binding to Talin Are Mutually Exclusive and Regulate Adhesion Assembly and Turnover. *J. Biol. Chem.* **2013**, *288*, 8238−8249.

(17) Grashoff, C.; Hoffman, B. D.; Brenner, M. D.; Zhou, R. B.; Parsons, M.; Yang, M. T.; McLean, M. A.; Sligar, S. G.; Chen, C. S.; Ha, T.; Schwartz, M. A. Measuring Mechanical Tension across Vinculin Reveals Regulation of Focal Adhesion Dynamics. *Nature* **2010**, *466*, 263−U143.

(18) Lee, H. S.; Lim, C. J.; Puzon-McLaughlin, W.; Shattil, S. J.; Ginsberg, M. H. Riam Activates Integrins by Linking Talin to Ras Gtpase Membrane-Targeting Sequences. *J. Biol. Chem.* **2009**, *284*, 5119−5127.

(19) Sun, N.; Critchley, D. R.; Paulin, D.; Li, Z. L.; Robson, R. M. Identification of a Repeated Domain within Mammalian Alpha-Synemin That Interacts Directly with Talin. *Exp. Cell Res.* **2008**, *314*, 1839−1849.

(20) Li, G. R.; Du, X. L.; Vass, W. C.; Papageorge, A. G.; Lowy, D. R.; Qian, X. L. Full Activity of the Deleted in Liver Cancer 1 (Dlc1) Tumor Suppressor Depends on an Ld-Like Motif That Binds Talin and Focal Adhesion Kinase (Fak). *Proc. Natl. Acad. Sci. U. S. A.* **2011**, *108*, 17129−17134.

(21) Popa, I.; Berkovich, R.; Alegre-Cebollada, J.; Badilla, C. L.; Rivas-Pardo, J. A.; Taniguchi, Y.; Kawakami, M.; Fernandez, J. M. Nanomechanics of Halotag Tethers. *J. Am. Chem. Soc.* **2013**, *135*, 12762−12771.

(22) Popa, I.; Kosuri, P.; Alegre-Cebollada, J.; Garcia-Manyes, S.; Fernandez, J. M. Force Dependency of Biochemical Reactions Measured by Single-Molecule Force-Clamp Spectroscopy. *Nat. Protoc.* **2013**, *8*, 1261−1276.

(23) Rivas-Pardo, J. A.; Alegre-Cebollada, J.; Ramirez-Sarmiento, C. A.; Fernandez, J. M.; Guixe, V. Identifying Sequential Substrate Binding at the Single-Molecule Level by Enzyme Mechanical Stabilization. *ACS Nano* **2015**, *9*, 3996−4005.
(24) Ainavarapu, R. K.; Brujic, J.; Huang, H. H.; Wiita, A. P.; Lu, H.; Li, L. W.; Walther, K. A.; Carrion-Vazquez, M.; Li, H. B.; Fernandez, J. M. Contour Length and Refolding Rate of a Small Protein Controlled by Engineered Disulfide Bonds. *Biophys. J.* **2007**, *92*, 225−233.
(25) Craig, D.; Gao, M.; Schulten, K.; Vogel, V. Tuning the Mechanical Stability of Fibronectin Type Iii Modules through Sequence Variations. *Structure* **2004**, *12*, 21−30.
(26) Gingras, A. R.; Ziegler, W. H.; Bobkov, A. A.; Joyce, M. G.; Fasci, D.; Himmel, M.; Rothemund, S.; Ritter, A.; Grossmann, J. G.; Patel, B.; Bate, N.; Goult, B. T.; Emsley, J.; Barsukov, I. L.; Roberts, G. C. K.; Liddington, R. C.; Ginsberg, M. H.; Critchley, D. R. Structural Determinants of Integrin Binding to the Talin Rod. *J. Biol. Chem.* **2009**, *284*, 8866−8867.
(27) Zhang, H.; Chang, Y.-C.; Huang, Q.; Brennan, M. L.; Wu, J. Structural and Functional Analysis of a Talin Triple-Domain Module Suggests an Alternative Talin Autoinhibitory Configuration. *Structure* **2016**, *24*, 721−729.
(28) Goult, B. T.; Bate, N.; Anthis, N. J.; Wegener, K. L.; Gingras, A. R.; Patel, B.; Barsukov, I. L.; Campbell, I. D.; Roberts, G. C. K.; Critchley, D. R. The Structure of an Interdomain Complex That Regulates Talin Activity. *J. Biol. Chem.* **2009**, *284*, 15097−15106.
(29) Margadant, F.; Chew, L. L.; Hu, X.; Yu, H.; Bate, N.; Zhang, X.; Sheetz, M. Mechanotransduction *in Vivo* by Repeated Talin Stretch-Relaxation Events Depends Upon Vinculin. *PLoS Biol.* **2011**, *9*, e1001223.
(30) Liu, J. R.; Wang, Y. L.; Goh, W. I.; Goh, H.; Baird, M. A.; Ruehland, S.; Teo, S.; Bate, N.; Critchley, D. R.; Davidson, M. W.; Kanchanawong, P. Talin Determines the Nanoscale Architecture of Focal Adhesions. *Proc. Natl. Acad. Sci. U. S. A.* **2015**, *112*, E4864−E4873.
(31) Wang, X. F.; Ha, T. Defining Single Molecular Forces Required to Activate Integrin and Notch Signaling. *Science* **2013**, *340*, 991−994.
(32) Roein-Peikar, M.; Xu, Q.; Wang, X. F.; Ha, T. Ultrasensitivity of Cell Adhesion to the Presence of Mechanically Strong Ligands. *Phys. Rev. X* **2016**, *6*, 9.
(33) Forscher, P.; Smith, S. J. Actions of Cytochalasins on the Organization of Actin-Filaments and Microtubules in a Neuronal Growth Cone. *J. Cell Biol.* **1988**, *107*, 1505−1516.
(34) Merkel, R.; Nassoy, P.; Leung, A.; Ritchie, K.; Evans, E. Energy Landscapes of Receptor-Ligand Bonds Explored with Dynamic Force Spectroscopy. *Nature* **1999**, *397*, 50−53.
(35) Carisey, A.; Tsang, R.; Greiner, A. M.; Nijenhuis, N.; Heath, N.; Nazgiewicz, A.; Kemkemer, R.; Derby, B.; Spatz, J.; Ballestrem, C. Vinculin Regulates the Recruitment and Release of Core Focal Adhesion Proteins in a Force-Dependent Manner. *Curr. Biol.* **2013**, *23*, 271−281.
(36) Durkin, M. E.; Yuan, B. Z.; Zhou, X.; Zimonjic, D. B.; Lowy, D. R.; Thorgeirsson, S. S.; Popescu, N. C. Dlc-1: A Rho Gtpase-Activating Protein and Tumour Suppressor. *J. Cell. Mol. Med.* **2007**, *11*, 1185−1207.
(37) Kim, T.; Vigil, D.; Der, C.; Juliano, R. Role of Dlc-1, a Tumor Suppressor Protein with Rhogap Activity, in Regulation of the Cytoskeleton and Cell Motility. *Cancer Metastasis Rev.* **2009**, *28*, 77−83.
(38) Lee, H. S.; Anekal, P.; Lim, C. J.; Liu, C. C.; Ginsberg, M. H. Two Modes of Integrin Activation Form a Binary Molecular Switch in Adhesion Maturation. *Mol. Biol. Cell* **2013**, *24*, 1354−1362.
(39) Klapholz, B.; Herbert, S. L.; Wellmann, J.; Johnson, R.; Parsons, M.; Brown, N. H. Alternative Mechanisms for Talin to Mediate Integrin Function. *Curr. Biol.* **2015**, *25*, 847−857.
(40) Golji, J.; Mofrad, M. R. K. The Talin Dimer Structure Orientation Is Mechanically Regulated. *Biophys. J.* **2014**, *107*, 1802−1809.
(41) Johnson, C. P.; Tang, H. Y.; Carag, C.; Speicher, D. W.; Discher, D. E. Forced Unfolding of Proteins within Cells. *Science* **2007**, *317*, 663−666.
(42) Yonemura, S.; Wada, Y.; Watanabe, T.; Nagafuchi, A.; Shibata, M. Alpha-Catenin as a Tension Transducer That Induces Adherens Junction Development. *Nat. Cell Biol.* **2010**, *12*, 533−U35.
(43) Haining, A. W. M.; Lieberthal, T. J.; del Río Hernández, A. Talin: A Mechanosensitive Molecule in Health and Disease. *FASEB J.* **2016**, *30*, 2073.
(44) Monkley, S. J.; Kostourou, V.; Spence, L.; Petrich, B.; Coleman, S.; Ginsberg, M. H.; Pritchard, C. A.; Critchley, D. R. Endothelial cell talin1 is essential for embryonic angiogenesis. *Dev. Biol.* **2011**, *349*, 494−502.
(45) Hutter, J. L.; Bechhoefer, J. Calibration of Atomic-Force Microscope Tips. *Rev. Sci. Instrum.* **1993**, *64*, 1868−1873.
(46) Butt, H. J.; Jaschke, M. Calculation of Thermal Noise in Atomic-Force Microscopy. *Nanotechnology* **1995**, *6*, 1−7.
(47) Berendsen, H. J. C.; Vanderspoel, D.; Vandrunen, R. Gromacs - a Message-Passing Parallel Molecular-Dynamics Implementation. *Comput. Phys. Commun.* **1995**, *91*, 43−56.
(48) Lindahl, E.; Hess, B.; van der Spoel, D. Gromacs 3.0: A Package for Molecular Simulation and Trajectory Analysis. *J. Mol. Model* **2001**, *7*, 306−317.
(49) Humphrey, W.; Dalke, A.; Schulten, K. Vmd: Visual Molecular Dynamics. *J. Mol. Graphics* **1996**, *14*, 33−38.

DOI: 10.1021/acsnano.6b01658
ACS Nano 2016, 10, 6648−6658